Available online at www.sciencedirect.com
ScienceDirect
Trans. Nonferrous Met. Soc. China 32(2022) 3663−3678
Transactions of Nonferrous Metals Society of China
www.tnmsc.cn

Improving electrochemical performance of Ni-rich layered oxide cathodes via one-step dual modification strategy

Yuan-lin CAO, Xiu-kang YANG, Lu WANG, Ling XIAO, Ni FU, Li ZOU,
Wen-bo MA, Zhe-ting LIU, Xiao-qin WANG, Li LIU, Hong-bo SHU, Xian-you WANG

Key Laboratory of Environmentally Friendly Chemistry and Applications of Ministry of Education,
National Base for International Science & Technology Cooperation,
Hunan Province Key Laboratory for Electrochemical Energy Storage and Conversion,
School of Chemistry, Xiangtan University, Xiangtan 411105, China

Received 9 September 2021; accepted 14 February 2022

Abstract: A one-step overall strategy from surface to bulk was proposed to simultaneously synthesize the Nb-doped and $LiNbO_3$-coated $LiNi_{0.83}Co_{0.12}Mn_{0.05}O_2$ cathode materials. The incorporation of $LiNbO_3$ coating can regulate the interface and facilitate the diffusion of Li-ions. Simultaneously, the stronger Nb—O bond can effectively suppress Li^+/Ni^{2+} cation mixing and strengthen the stability of crystal structure, which helps to mitigate the anisotropic variations of lattice parameters during Li^+ de/intercalation. The results showed that the dual-modified materials exhibited good structural stability and distinguished electrochemical performance. The optimal NCM-Nb2 sample showed an excellent capacity retention of 90.78% after 100 cycles at 1*C* rate between 2.7 and 4.3 V, while only 67.90% for the pristine one. Meanwhile, it displayed a superior rate capability of 149.1 mA·h/g at the 10*C* rate. These results highlight the feasibility of one-step dual modification strategy to synchronously improve the electrochemical performance of Ni-rich layered oxide cathodes.

Key words: Ni-rich cathodes; niobium; one-step strategy; dual modification; structural stability; electrochemical performance

1 Introduction

In recent years, as energy and environmental issues have become increasingly severe, the search for alternative renewable energy has become a hot spot of social concern. Due to their high energy storage and conversion efficiency, Li-ion batteries (LIBs) are widely used in many fields from portable electronics to electric vehicles (EV) since they were successfully commercialized by Sony in 1990 [1,2]. The current commercialized cathode materials mainly include $LiCoO_2$, $LiMn_2O_4$, $LiFePO_4$ and ternary NCM/NCA. Especially, nickel-rich ternary layered material ($LiNi_xCo_yMn_zO_2$, $x\geq0.6$) is regarded to be one of the most commercially valuable members due to its high energy density [3−6]. Although the discharge specific capacity significantly rises with the expansion in the proportion of nickel, new problems will also follow, such as cation mixing, surface structure degradation and microcrack generation [7−9]. Since the ion radii of Ni^{2+} (0.069 nm) and Li^+ (0.076 nm) are approximately similar, Ni^{2+} ions tend to occupy the lithium layer, resulting in the increase of cation mixing degree [10]. Meanwhile, in the deep delithiation state, the high-valence Ni^{4+} at the particle interface has strong oxidizing property which is easy to react with the electrolyte. Eventually, it will induce degradation of the surface

Corresponding author: Xiu-kang YANG, Tel: +86-15898511615, E-mail: yshowk23@163.com
DOI: 10.1016/S1003-6326(22)66047-3

structure from the layered phase ($R\bar{3}m$) to the disordered spinel-like ($Fd\bar{3}m$) and rock-salt phase ($Fm\bar{3}m$) [11]. Besides, the repeated H2−H3 phase transition that occurs in the deep delithiated state (≥4.2 V) is usually accompanied by rapid and dramatic changes in lattice parameters and the generation of anisotropic strain, which eventually leads to the generation of microcracks [12]. The newly generated microcracks are exposed to the electrolyte, further increasing interfacial side reactions. Thus, it would increase the impedance of electrode and reduce the dynamic performance, and even cause the powdering of cathode material.

In order to overcome the aforementioned shortcomings, researchers have carried out extensive efforts. Among a wide range of modification strategies, surface coating is a very practical solution [13,14]. At present, the reported coating materials mainly include metal oxides (Al_2O_3 [15], Y_2O_3 [16], V_2O_5 [17]), fluorides (LiF [18], MgF_2 [19], AlF_3 [20]), phosphates (Li_3PO_4 [21], $AlPO_4$ [22], $Mn_3(PO_4)_2$ [23]), and fast ionic conductors ($Li_4Ti_5O_{12}$ [24], Li_2ZrO_3 [25], $Li_{1.3}Al_{0.3}Ti_{1.7}(PO_4)_3$ [26], Li_4SiO_4 [27]). These coating media can act as a protective barrier to effectively alleviate interfacial side reactions, thereby improving the surface stability. However, the surface coating strategy only affects the surface properties of the material, and bulk structure is also vital to electrochemical performance of cathode materials. Therefore, bulk doping is considered as another effective method to improve material properties as well. For elemental substitution, various dopants such as Mg [28], Ta [29], B [30] and W [31], have been adopted to effectively strengthen the stability of the crystal structure of Ni-rich cathode materials, by decreasing Li^+/Ni^{2+} anti-site defects and slowing down anisotropic volume deformation.

To more effectively enhance the overall structural stability of Ni-rich cathode materials, it is essential to comprehensively consider the structural modification from surface to bulk [32]. Although there are quite a few such literature reports, most of them adopt a two-step method, that is, the doped Ni-rich layered cathode material is firstly prepared and then coated on the surface. Due to the sensitivity of Ni-rich cathode materials to air and moisture, these methods not only have a complex process but also require a strict operating environment. Thence, it is extremely necessary to develop a feasible strategy to synchronously consolidate the overall structural stability from surface to bulk.

Herein, we develop an overall structural modification strategy from surface to bulk via a facial one-step wet chemical method. This strategy simultaneously integrates $LiNbO_3$ surface coating and Nb^{5+} ion doping for Ni-rich layered cathode materials, as illustrated in Fig. 1. The

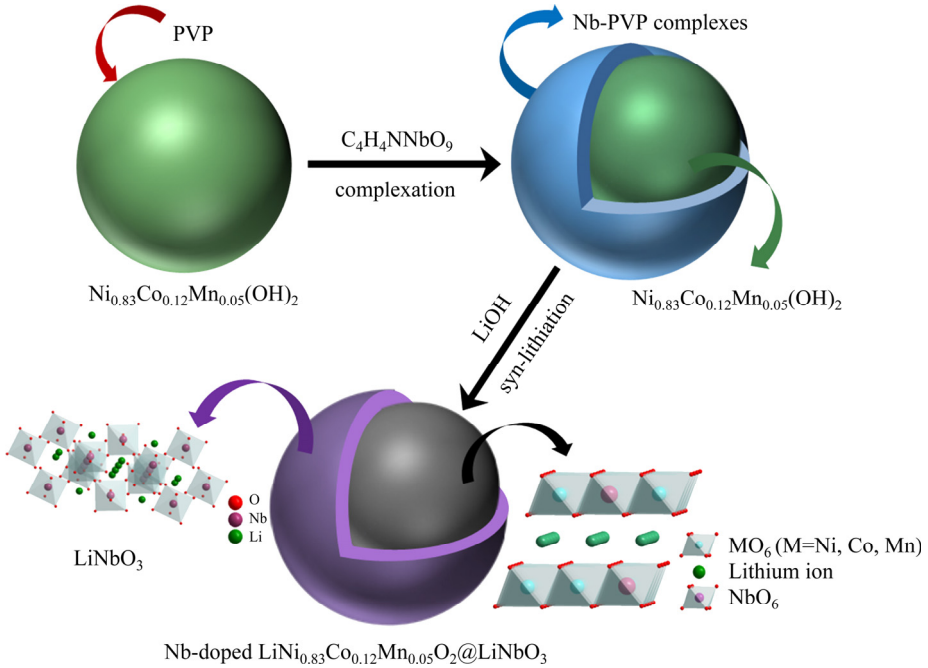

Fig. 1 Schematic diagram of synthesis process of dual-modified cathode materials (PVP−polyvinylpyrrolidone)

electrochemically stable $LiNbO_3$ coating can greatly reduce adverse interface side reactions to enhance surface structural stability. Moreover, $LiNbO_3$ is also an effective ion conductor which can offer a moderate Li-ion conductivity of 1×10^{-5} S/cm at room temperature. Furthermore, the stronger Nb−O bond dissociation energy (ΔH_{f298}(Nb—O)= 753 kJ/mol) is expected to effectively suppress Li^+/Ni^{2+} cation mixing and stabilize crystal structure [33]. With the improved overall structural stability attributed to the synergistic effect of $LiNbO_3$ surface coating and Nb^{5+} ion doping, as expected, the dual-modified Ni-rich layered cathode material enhances the electrochemical performance.

2 Experimental

2.1 Material synthesis

To synthesize the bare $LiNi_{0.83}Co_{0.12}Mn_{0.05}O_2$ material for comparison, commercial $Ni_{0.83}Co_{0.12}Mn_{0.05}(OH)_2$ precursors were mixed with $LiOH\cdot H_2O$ with an appropriate mole ratio of Li:TM=1.05:1. Subsequently, the mixed powders were preheated to 500 °C for 6 h, and then calcined at 780 °C for 12 h at a heating rate of 3 °C/min under O_2 atmosphere. The obtained Ni-rich layered sample was denoted as pristine NCM.

To prepare the modified $LiNi_{0.83}Co_{0.12}Mn_{0.05}O_2$ samples, firstly, a certain stoichiometric amount of PVP was added to a certain volume of anhydrous ethanol and stirred to fully dissolve. Then, 1 g of commercial $Ni_{0.83}Co_{0.12}Mn_{0.05}(OH)_2$ precursor powders were slowly added and evenly scattered for 6 h. Subsequently, an anhydrous ethanol solution containing a specific stoichiometric amount of $C_4H_4NNbO_9\cdot xH_2O$ (analytical grade) was added dropwise into the above dispersed mixture at a rate of 15 mL/h with vigorous stirring. Afterwards, the resulting suspension was further continuously stirred at 65 °C under a speed of 650 r/min until the solvent was completely evaporated to form the Nb-PVP coated $Ni_{0.83}Co_{0.12}Mn_{0.05}(OH)_2$ precursor. Finally, under the above conditions, dried powder materials were blended with $LiOH\cdot H_2O$ and then sintered to acquire dual-modified $LiNi_{0.83}Co_{0.12}Mn_{0.05}O_2$ samples (denoted as NCM-Nb1, NCM-Nb2, NCM-Nb3, and NCM-Nb5, respectively, which correspond to the Nb_2O_5 proportions of 1, 2, 3, and 5 wt.% of $Ni_{0.83}Co_{0.12}Mn_{0.05}(OH)_2$ precursors in sequence.)

2.2 Material characterization

The crystal structure was confirmed by powder X-ray diffraction (XRD, Bruker D8 Advance, using Cu K_α radiation) analysis at a scanning rate of 5 (°)/min. The surface morphology was examined by employing scanning electron microscopy (SEM, JEOL, JSM−6610LV), and the surface micro-structure and main element distribution of the samples were characterized by transmission electron microscopy (TEM, FEI, JEM2010). The chemical state of the surface elements of the samples was investigated by X-ray photoelectron spectroscopy (XPS, K-Alpha 1063). The thermal stability was determined by differential scanning calorimetry (DSC, TAQ2000) after the activated Li-ion cell including cathode materials was fully charged to 4.3 V (vs Li^+/Li).

2.3 Electrochemical measurement

To evaluate the electrochemical performances of as-synthesized cathode materials, CR2025 coin-type cells were adopted. The cathode slurries were made by mixing the as-prepared materials with conductive carbon black (Super-P) and polyvinylidene fluoride (PVDF) at the mass ratio of 8:1:1, followed by adding an appropriate amount of N-methyl pyrrolidone (NMP) as a dispersant. After fully stirring, the slurries were evenly coated on an aluminum foil and fully dried at 90 °C, and then cut into round pieces with an active material loading confined within ~2 mg/cm^2. Subsequently, the cells containing the prepared electrode, lithium metal counter electrode, porous polypropylene membrane (Celgard2325) and electrolyte (1 mol/L $LiPF_6$, EC/DMC/EMC 1:1:1, volume ratio) were assembled in a glove box (MIKROUNA, Super (1220/750/900), Germany) filled with argon. Galvanostatic charge and discharge measurements were performed by employing various current densities (1C=200 mA/g) (Neware battery test system, BT−9300) at 25 °C in a specific voltage range (vs Li^+/Li). Cyclic voltammetry (CV) at a sweeping speed of 0.1 mV/s and electrochemical impedance spectroscopy (EIS) with the frequency range of 0.01 Hz to 100 kHz were conducted by employing electrochemical workstation (CHI660E, Shanghai, Chenhua). Galvanostatic intermittent titration technique (GITT) tests were performed through a battery testing system (Neware, BT−9300). The constant current (0.1C) pulse and

relaxation time of a single titration step were 10 and 60 min, respectively.

3 Results and discussion

3.1 Structure, morphology and surface chemistry characteristics

XRD tests were performed to characterize the crystal structure of the pristine NCM, NCM-Nb1, NCM-Nb2, NCM-Nb3, and NCM-Nb5 samples. Figure 2(a) shows the XRD patterns of the as-prepared samples. As can be observed, all the samples can be indexed to the α-$NaFeO_2$ layered hexagonal structure corresponding to the $R\bar{3}m$ space group (PDF#87-1562). Close observation revealed that the NCM-Nb5 sample had an additional weak diffraction peak at 2θ of around 23°, which belonged to the (012) plane of $LiNbO_3$ (PDF#20-0631). The existence of $LiNbO_3$ peaks was not found in other modified samples due to the low content of Nb. Additionally, compared to the pristine NCM sample, the (003) reflection of the modified samples slightly shifted to a lower 2θ value, which can be clearly seen in Fig. 2(b). With the increase of Nb content, the peak position continues to move to a low angle. It can be inferred that part of Nb^{5+} ions penetrate into the crystal lattice of Ni-rich layered oxides resulting in the enlarged cell parameters, owing to the larger radius of Nb^{5+} (0.64 Å) than that of Ni^{3+} (0.56 Å), Co^{3+} (0.545 Å) and Mn^{4+} (0.53 Å) [34−36]. For the pristine NCM, NCM-Nb1 and NCM-Nb2 samples, the apparent splitting of (006)/(102) and (108)/(110) pairs revealed a well-ordered layer structure. But for the NCM-Nb3 and NCM-Nb5 samples, the splitting degree of (108)/(110) peaks was not obvious, which may be due to the increase of mixing degree caused by excessive high-valence cation doping [37].

The XRD Rietveld refinement of pristine NCM and NCM-Nb2 is shown in Fig. 2(c), and the corresponding lattice parameters are listed in Table 1. Generally, the ratio of $I(003)/I(104)$ can reflect the ordered degree of the layered characteristics of Ni-rich oxides. For the NCM-Nb2 sample, it shows a higher $I(003)/I(104)$ intensity ratio than the

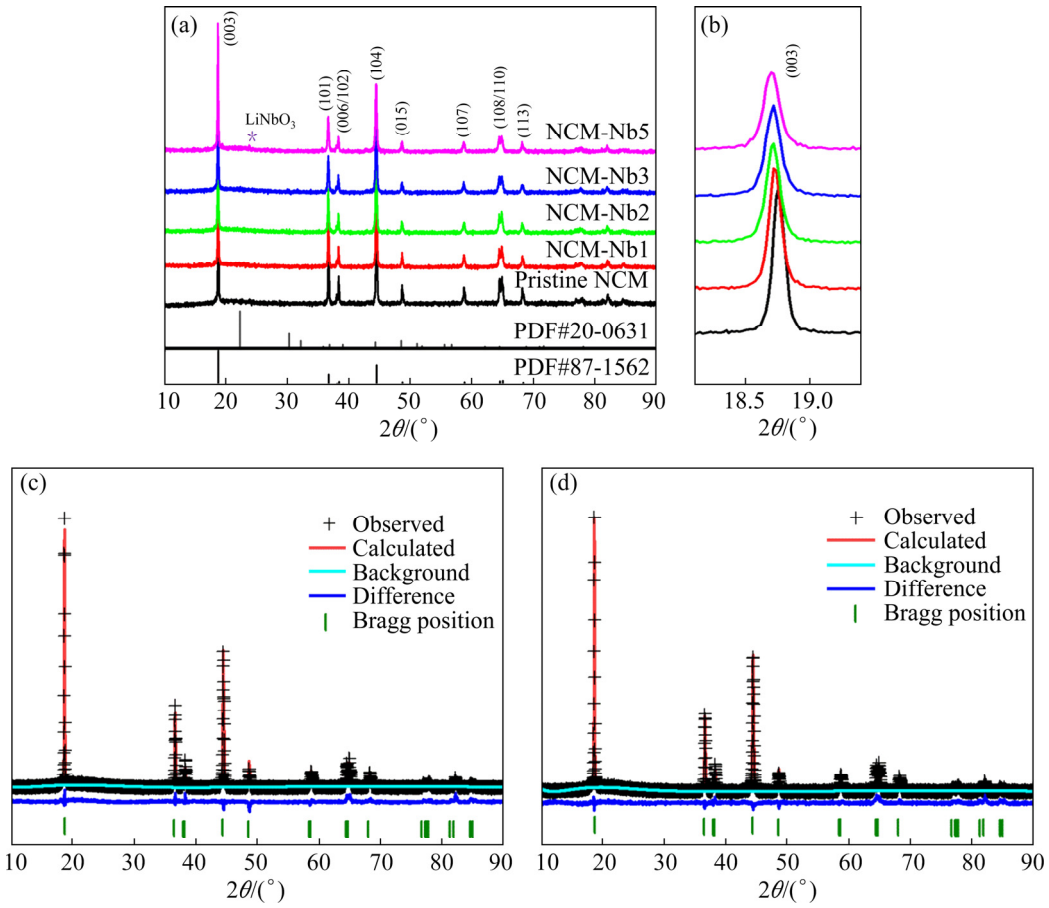

Fig. 2 XRD patterns of as-prepared Ni-rich layered cathode materials (a), magnified regions (b) taken from corresponding XRD patterns in (a), and Rietveld refinement results of XRD patterns of pristine NCM (c) and NCM-Nb2 (d)

pristine NCM, which is probably due to the stronger Nb—O bond that is able to strengthen TM−O slabs to hinder the migration of TM ions into Li slabs [38]. In addition, based on the Rietveld refinement results in Table 1, the lattice parameters of the NCM-Nb2 sample have also increased relatively attributed to Nb^{5+} doping with larger ion radius. Therefore, it can be fully inferred that the expanded lattice parameters in the NCM-Nb2 sample will facilitate the electrochemical de/intercalation of Li^+ ions.

SEM examination was used to characterize the effect of dual modification on the surface morphology of raw materials. Figure 3 displays the SEM images of the pristine NCM, NCM-Nb1, NCM-Nb2 and NCM-Nb3 samples. All the as-prepared materials exhibit the overall morphology of spherical secondary micro-particles of 6−8 μm, which are composed of abundant aggregated nano-scale primary grains. Through further comparison, it can be seen that the edges and corners of the primary particles on the surface of the pristine NCM material are clearly visible, while that of the modified materials becomes blurred as the niobium content increases. At the same time, the surface of the modified materials becomes relatively rough. These changes in surface morphology fully demonstrate that $LiNbO_3$ is successfully formed on the surface of the material particles after Nb modification.

To further characterize the microstructure of the as-synthesized cathode materials, TEM and high-resolution TEM (HRTEM) examinations were performed. The image of the pristine NCM particles from bulk to surface presents an apparent interplanar spacing of 0.204 nm shown in Fig. 4(a), which is identical to the (104) crystal plane of the layered $R\bar{3}m$ structure. Furthermore, it can be further verified by the fast Fourier transform (FFT) patterns in the block diagrams (1) and (2), where the (104) plane diffraction spots are coherent with the $R\bar{3}m$ space group. On the contrary, the NCM-

Table 1 Lattice parameters of pristine NCM and NCM-Nb2 by Rietveld refinement

Sample	Lattice parameter				Reliability factor			
	a/Å	c/Å	c/a	Volume/Å^3	$I_{(003)}/I_{(104)}$	R_{wp}/%	R_p/%	χ^2
Pristine NCM	2.8701	14.1815	4.9411	101.16	1.707	5.67	4.03	3.36
NCM-Nb2	2.8717	14.1943	4.9428	101.37	2.039	4.92	3.64	2.52

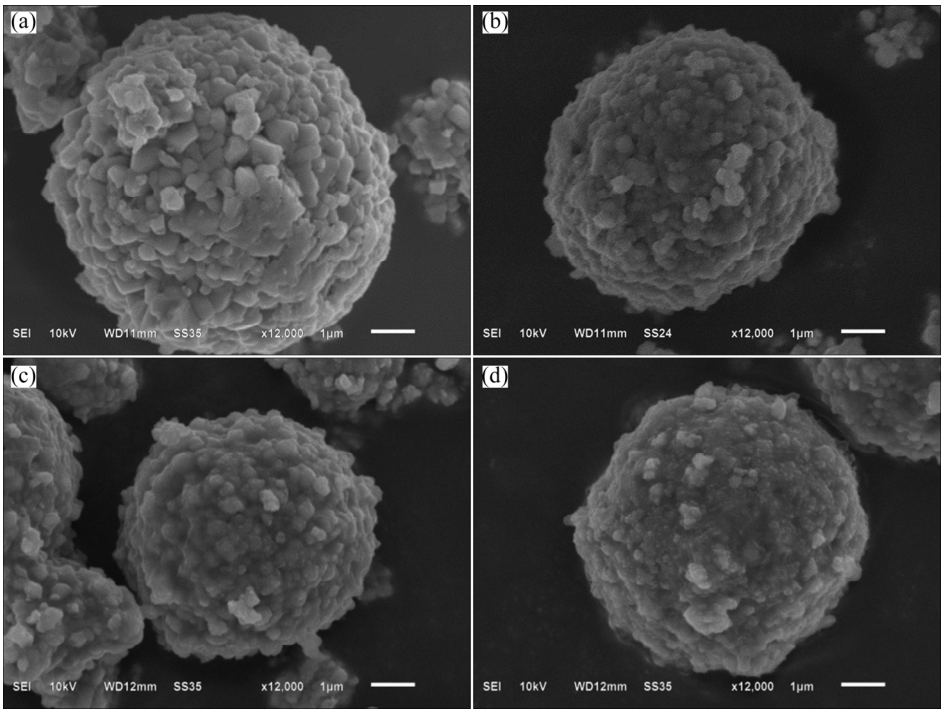

Fig. 3 SEM images of as-prepared Ni-rich layered cathode materials: (a) Pristine NCM; (b) NCM-Nb1; (c) NCM-Nb2; (d) NCM-Nb3

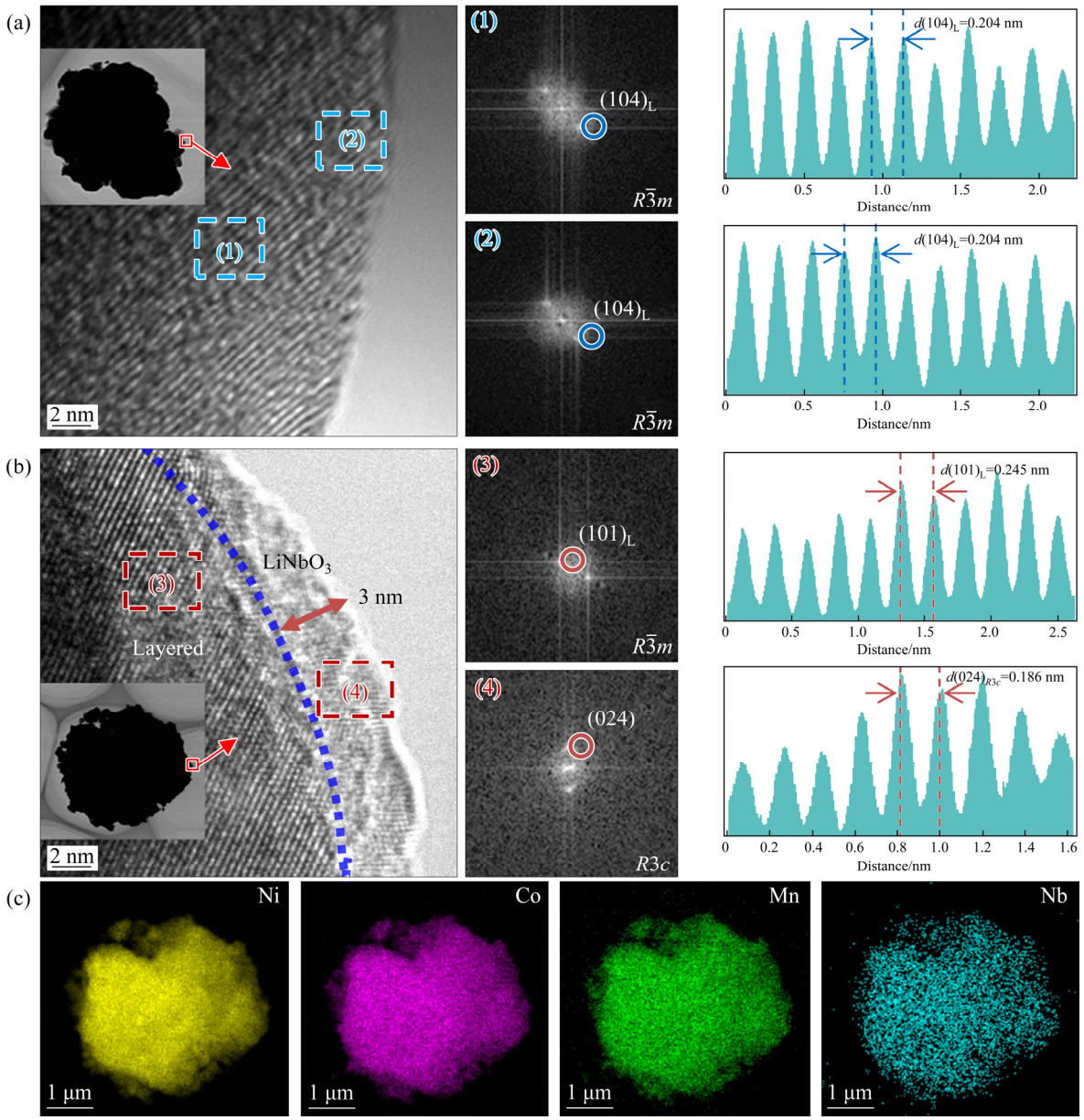

Fig. 4 TEM, HRTEM images and corresponding FFT images of pristine NCM (a) and NCM-Nb2 (b), and elemental mapping of NCM-Nb2 (c)

Nb2 particles reveal a clear core–shell structure in Fig. 4(b), where the core is tightly connected with a uniform coating layer with a thickness of approximately 3 nm. Meanwhile, it shows two distinct sets of lattice fringes. The interplanar spacing of 0.245 nm in the block diagram (3) and 0.186 nm in the block diagram (4) are ascribed to the (101) plane of the bulk layered phase and the (024) plane of the $LiNbO_3$ surface phase, respectively, as illustrated in the corresponding FFT patterns. Form these results, it can be inferred that the strong interaction between the $LiNbO_3$ coating and the host cathode material is expected to improve the interface stability to a certain extent.

In addition, the corresponding EDS elemental mapping was adopted to explore the distribution of main elements on the surface of the NCM-Nb2 particles. Through Fig. 4(c), we can find that the distribution of all the detected elements including Nb is relatively coincident, confirming that the $LiNbO_3$ compound is homogeneously distributed on the surface of the NCM-Nb2 particles. These findings can persuasively illustrate that the $LiNbO_3$ coating can serve as a protective medium between the host material and the electrolyte.

The chemical states of the surface elements of

the pristine NCM and NCM-Nb2 samples were discussed by XPS analysis. The key binding energy peaks of Ni, Co, Mn and O were detected in both samples, whereas the binding energy peaks of Nb^{5+} could be merely found in the NCM-Nb2 sample (Figs. 5(a) and (f)). The divided parts of the Ni $2p_{3/2}$ spectrum shown in Fig. 5(b) at 854.6 and 855.8 eV can correspond to the binding energies of Ni^{2+} and Ni^{3+}, respectively. More importantly, through quantitative analysis based on peak area, we found that the proportion of Ni^{3+} in the both samples is relatively large. Interestingly, the molar ratio of Ni^{3+} to Ni^{2+} in NCM-Nb2 is slightly less than that in pristine NCM. It is reported that this phenomenon may be caused by a charge compensation mechanism resulting from part of Nb^{5+} ions diffusing into the

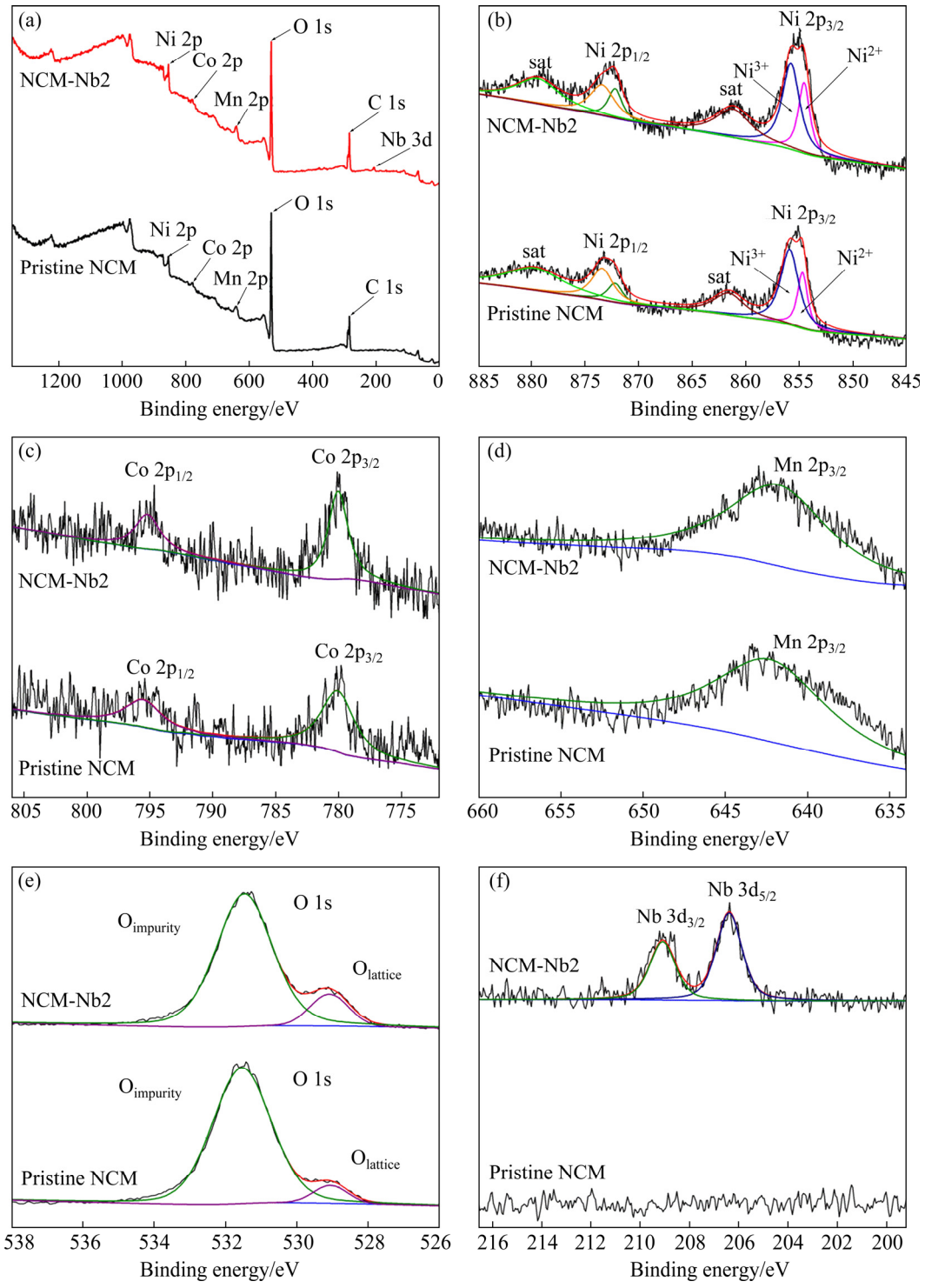

Fig. 5 XPS spectra of pristine NCM and NCM-Nb2 samples

bulk lattice of the cathode material after high temperature co-lithiation treatment, leading to the reduction in the oxidation state of Ni^{3+} ions [39]. Although there are slightly more Ni^{2+} ions, the stronger interaction between the Nb^{5+}-doped and O^{2-} ions can strengthen the TM−O layer to reduce the degree of Li^{+} /Ni^{2+} cation mixing [40], which is consistent with the XRD results. The Co 2p peaks in Fig. 5(c) are located at 795.2 and 780.1 eV, while the Mn $2p_{3/2}$ peaks in Fig. 5(d) are located at 642.3 eV, which are assigned to the +3 and +4 oxidation states of Co and Mn, separately. This result indicated that the Nb modification scarcely influences the chemical state of Co and Mn in Ni-rich cathode materials. The peaks located at 531.5 and 529.1 eV in Fig. 5(e) are ascribed to impurity oxygen and lattice oxygen, respectively. For NCM-Nb2, The ratio of O 1s peak area of impurity oxygen to lattice oxygen is smaller than that of pristine NCM, because there is a strong Nb—O bond between Nb^{5+}-doped and O^{2-} ions, signifying less surface lithium residues of NCM-Nb2 than that of pristine NCM. Less impurity oxygen means that the interface parasitic reactions that produce O_2, CO_2 and CO and cause serious safety issues are relatively reduced, thereby improving the structural stability of NCM-Nb2 [9,41]. In addition, it can be clearly observed in NCM-Nb2 that the binding energy peaks of Nb^{5+} at 209.5 and 206.3 eV in Fig. 5(f) correlated with Nb $3d_{3/2}$ and Nb $3d_{5/2}$, respectively, which implies the presence of Nb-containing compounds on the surface of dual-modified cathode materials.

3.2 Electrochemical and thermal performance

In order to explore the electrochemical properties of the as-synthesized materials, coin-type cells were assembled and tested. Figure 6(a) shows the initial charge–discharge profiles of pristine NCM, NCM-Nb1, NCM-Nb2 and NCM-Nb3 at 0.1*C* between 2.7 and 4.3 V. All samples display the same typical electrochemical reaction platform belonging to Ni-rich layered cathode material, showing that the $LiNbO_3$ coating layer is

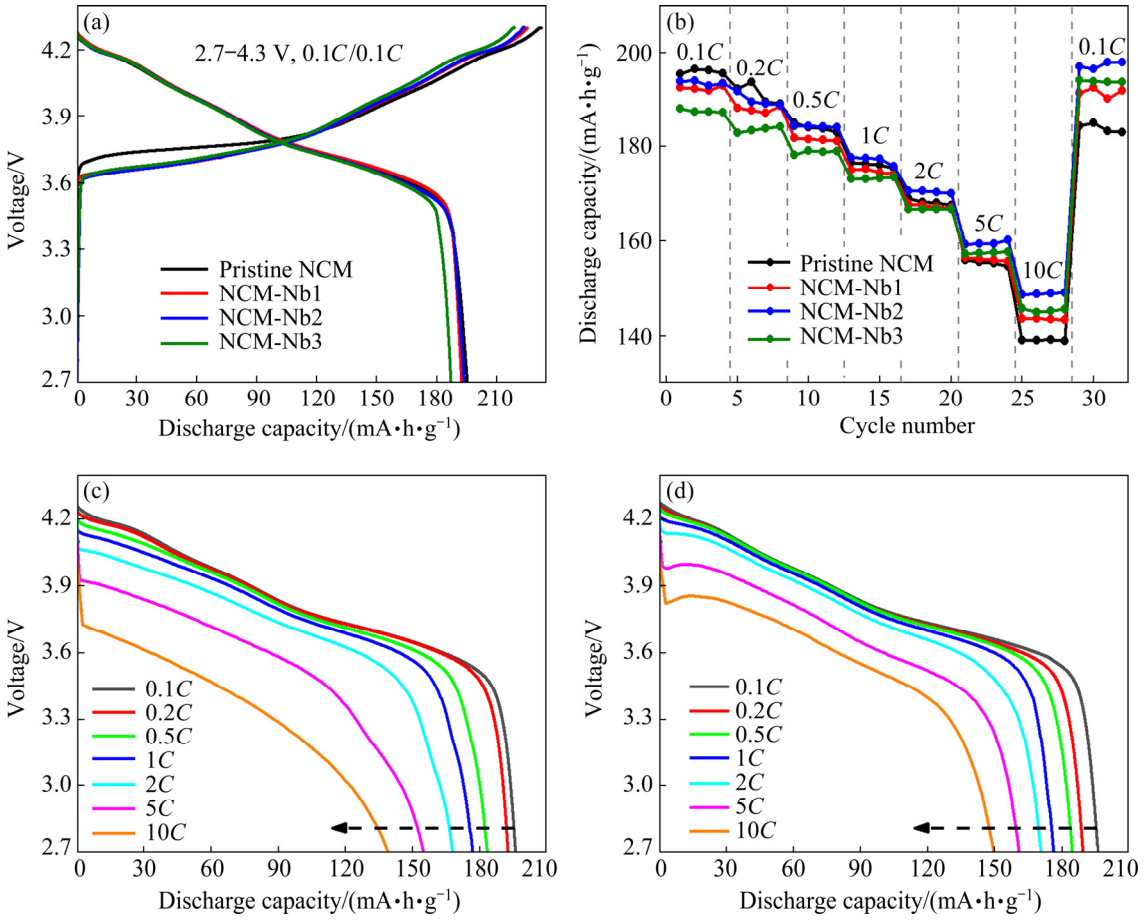

Fig. 6 Initial charge/discharge curves of as-synthesized materials (a), rate capability of as-synthesized materials by employing different current rates from 0.1*C* to 10*C* (b), and corresponding discharge profiles of pristine NCM (c) and NCM-Nb2 (d) at different rates

electrochemically inert within the above voltage range. It was observed that the first discharge capacities of pristine NCM, NCM-Nb1, NCM-Nb2 and NCM-Nb3 were 195.45, 192.53, 193.80 and 187.25 mA·h/g, respectively, showing a gradual downward trend with the increased addition amount of Nb element. This trend is due to the fact that $LiNbO_3$ is electrochemically inert, and a too thick coating layer hinders the transport of Li-ions at the electrode−electrolyte interface. Fortunately, the initial coulombic efficiency was slightly enhanced after Nb-modification. It might be attributed to that $LiNbO_3$ is not only a fast ion conductor, but also serves as a protective layer to retard adverse side reactions, thereby improving the reversibility of electrochemical reaction.

As demonstrated in Fig. 6(b), the rate capabilities of the as-synthesized materials were investigated by incrementally varying the current rate from 0.1*C* to 10*C* every four cycles between 2.7 and 4.3 V. It can be found that the reversible capacity of all the modified cathode materials is considerably higher than that of the pristine NCM material, especially at the ultra-high rate of 10*C*. The NCM-Nb2 cathode delivered the highest reversible specific capacity of 149.1 mA·h/g at the rate of 10*C*, while the pristine NCM only 139.2 mA·h/g. Besides, when the current density was restored to 0.1*C*, the value of the NCM-Nb2 can resume to 197.0 mA·h/g, confirming its superior high current withstand capability. Furthermore, it can be found from Figs. 6(c,d) that the discharge voltage plateau drop of the NCM-Nb2 cathode is evidently smaller than that of pristine NCM from 0.1*C* to 10*C*. Therefore, the results strongly proved that the dual-modified cathode materials had better Li^+ de/intercalation kinetics and structural stability than the pristine NCM.

The cycling performance of the obtained materials under different charging and discharging procedures is viewed in Fig. 7. The pristine NCM reached 187.3 mA·h/g in the 1st circle at 1*C* between 2.7 and 4.3 V, but the capacity retention after 100 cycles was only 67.90%. Although the initial cycle discharge capacity of the modified cathode materials is slightly lower than that of the

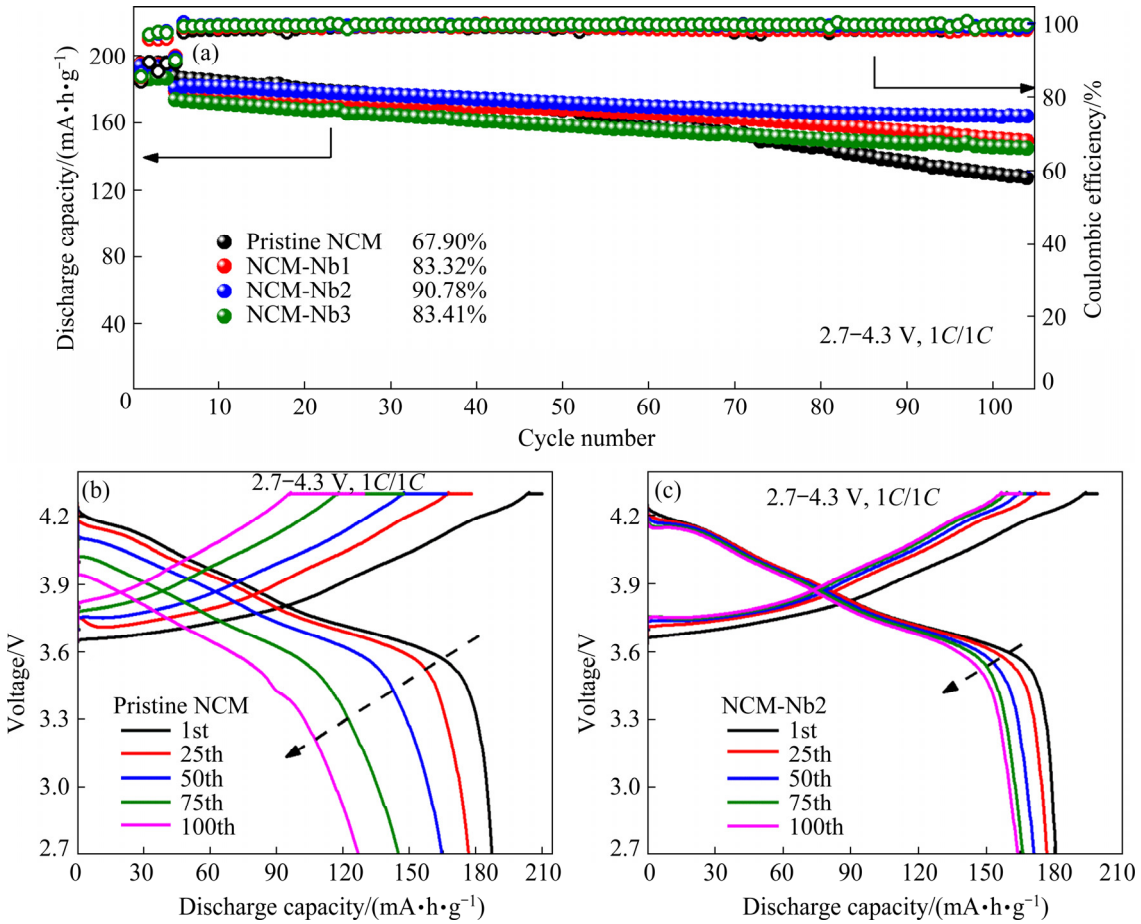

Fig. 7 Cycling performance of samples at 1*C* between 2.7 and 4.3 V (a), and corresponding charge−discharge plots of pristine NCM (b) and NCM-Nb2 (c)

pristine material, the capacity retention has been greatly improved. The retentions of NCM-Nb1, NCM-Nb2 and NCM-Nb3 after 100 cycles are 83.32%, 90.78% and 83.41%, respectively. Especially, the NCM-Nb2 sample has the highest retention. Figured 7(b) and (c) vividly depict their evolution of the corresponding charge−discharge plots after Nb modification, indicating that NCM-Nb2 maintains the slight voltage fading and polarization as the cycle progresses.

In addition, to further explore the stabilizing effect caused by dual modification, the pristine NCM and NCM-Nb2 electrodes were cycled at a high cut-off potential or an elevated rate. We can see from Fig. 8(a) that the capacity retention of NCM-Nb2 can reach 85.52% after 100 cycles at the high rate of 5*C*, obviously higher than that of pristine NCM (61.86%). Similarly, when the cut-off potential was increased to 4.5 V in Fig. 8(b), the specific capacity of NCM-Nb2 after 100 cycles was 152.86 mA·h/g, and its retention was 86.45%, while that of pristine NCM rapidly attenuated to 99.85 mA·h/g with a retention of merely 51.13%. The above results further confirmed that the dual-modified NCM samples exhibited improved Li^+ de/intercalation stability. This is mainly due to a uniform and tight ion conductive $LiNbO_3$ surface coating layer, which can effectively prevent from direct contact and mitigate detrimental side reactions between the active material and the electrolyte [42]. Moreover, the Nb^{5+} ion doping can also alleviate the irreversible structural changes of the crystal lattice because of the stronger Nb—O bond, and retain the stability of the crystal structure. Both can synergistically improve the overall structural stability of Ni-rich cathode materials from interface to bulk [43−46].

CV tests were conducted to discuss the electrochemical delithiation/lithiation process of the materials. Figure 9 illustrates the initial five cycles of CV profiles for the pristine NCM and NCM-Nb2 electrodes in the voltage range of 2.7−4.3 V (Figs. 9(a, b)) and 2.7−4.5 V (Figs. 9(c, d)). We can find three pairs of redox peaks which are designated as the phase transition from the first hexagonal phase (H1) to the monoclinic structure (M) and the next two other hexagonal structures (H2 and H3) [47]. As shown by the dotted rectangles, the anodic peak intensity of pristine NCM at a high potential of ~4.2 V continuously drops upon cycling, and is more pronounced at the higher cut-off voltage of 4.5 V, implying that H2−H3 irreversible

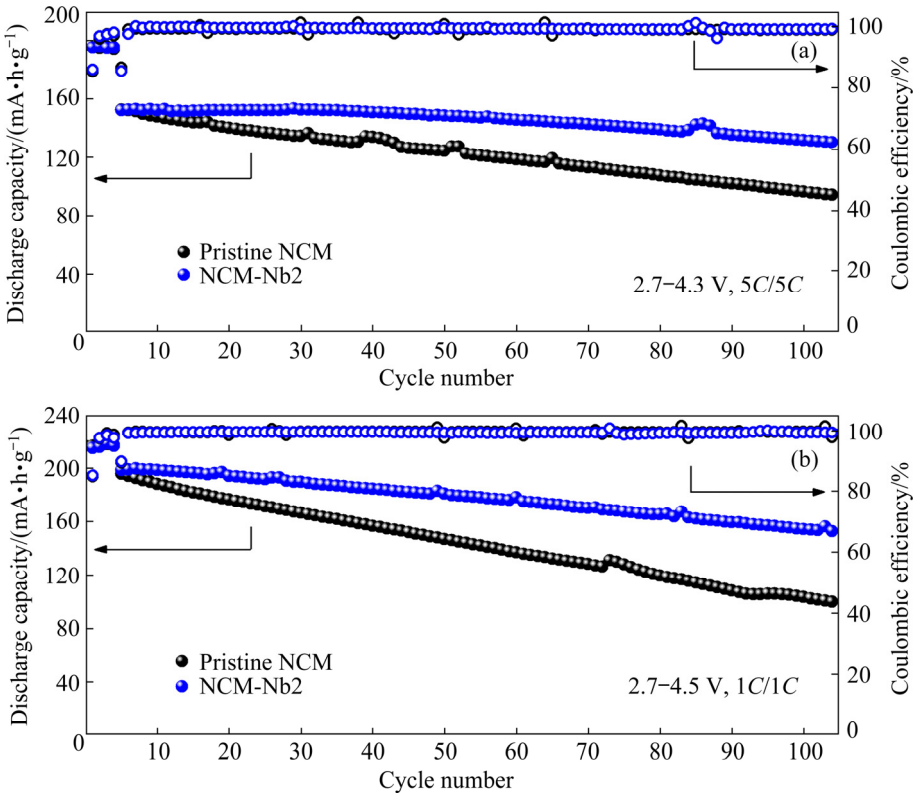

Fig. 8 Cycling performance of pristine NCM and NCM-Nb2 samples at ultra-high rate of 5*C* (a) and high cut-off voltage of 4.5 V (b)

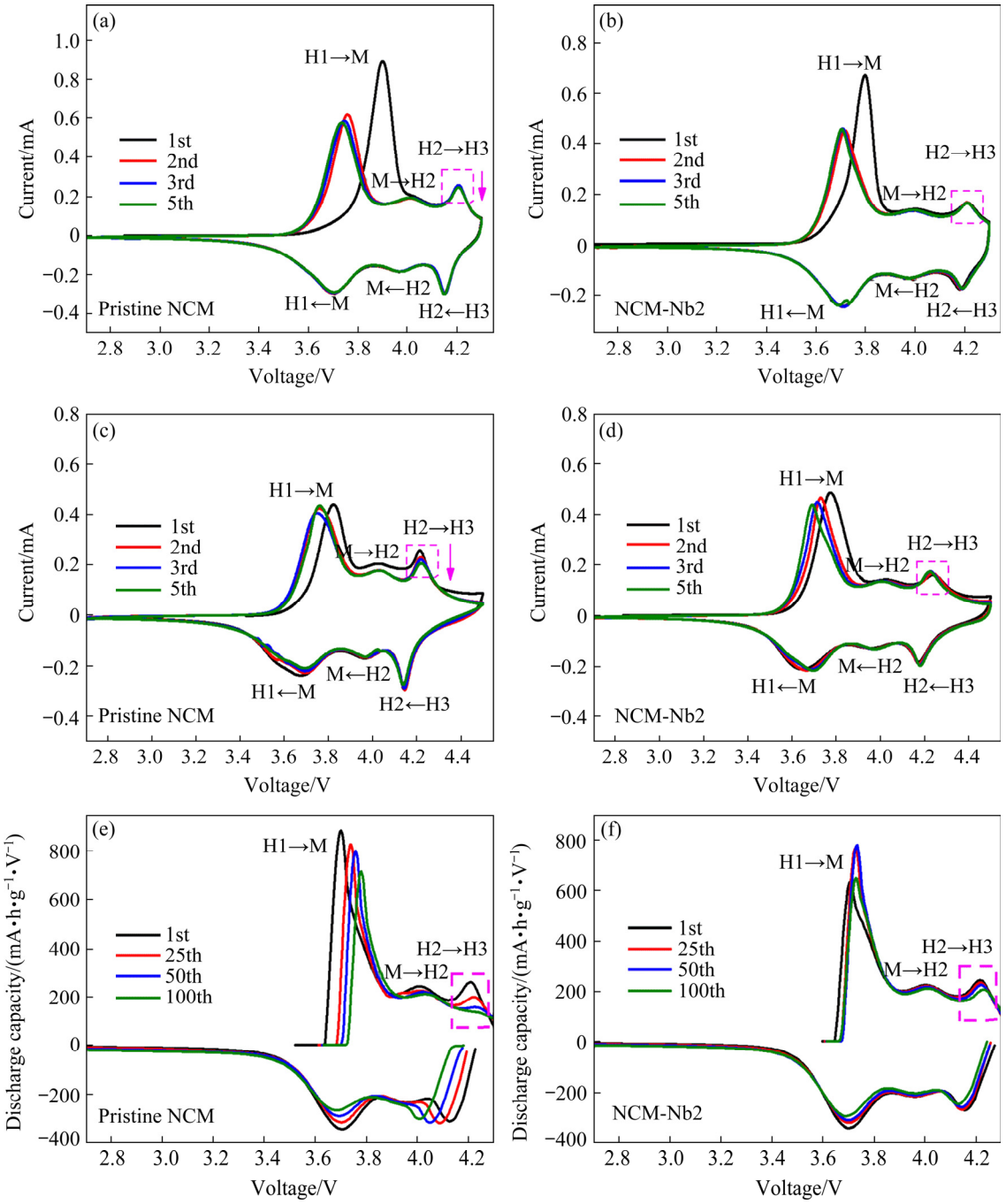

Fig. 9 Cyclic voltammetry curves of samples at scanning rate of 0.1 mV/s in voltage range of 2.7−4.3 V (a, b) and 2.7−4.5 V (c, d), and differential capacity curves of pristine NCM (e) and NCM-Nb2 (f) during cycling between 2.7 and 4.3 V at 1*C*

phase transition loss will eventually lead to capacity fading [48]. However, as the cycle progressed, the profiles of NCM-Nb2 basically overlapped, and the variation of peak intensities can be nearly ignored. In addition, dQ/dV profiles are also consistent with the cyclic voltammetry test results, and Figs. 9(e, f) display the 1st, 25th, 50th, and 100th cycles at 1*C* between 2.7−4.3 V for the pristine NCM and NCM-Nb2 cathodes. It also can be observed from the dotted rectangles that NCM-Nb2 basically maintains the peak intensity in the subsequent cycles, while it decreases evidently for pristine NCM until nearly disappears. The above results jointly indicate that H2−H3 irreversible phase transition can be suppressed to a certain extent by the dual modification strategy, thereby reducing the

structural degradation of Ni-rich layered oxides.

Galvanostatic intermittent titration technique (GITT) is a widely accepted method to effectively evaluate the Li^+ diffusion kinetics of electrode materials. Figures 10(a, b) depicted the GITT profiles of the pristine NCM and NCM-Nb2 cathodes. The apparent diffusion coefficient of Li^+ (D_{Li^+}) can be obtained by employing Eq. (1) [49]:

$$D_{Li^+}=\frac{4}{\pi\tau}\left(\frac{m_B V_m}{M_B S}\right)^2\left(\frac{\Delta E_s}{\Delta E_\tau}\right)^2\left(\tau\ll\frac{L^2}{D_{Li^+}}\right) \quad (1)$$

where m_B (g), M_B (g/mol) and V_m (cm^3/mol) are the mass, the molar mass and the volume of active materials, respectively; τ (s) is the applied current pulse time; S (cm^2) is the apparent surface of the cathode; L (cm) is the thickness of the cathode; ΔE_τ and ΔE_s represent the transient voltage change during the current pulse and the steady voltage change after the relaxation period, separately. The detailed description of a single titration step during the charging process is shown in Fig. 10(d).

Through the comparative analysis of the calculated apparent Li^+ diffusion coefficient curves in Fig. 10(c), it can be found that the D_{Li^+} of the pristine NCM and NCM-Nb2 electrodes has a gradually increasing trend until it is charged to approximately 3.7 V. It is due to the removal of Li-ions which causes the expansion of Li slab space and helps to promote the migration of Li-ions. Then the D_{Li^+} of the NCM-Nb2 cathode slowly increased and remained almost at a high level. However, the D_{Li^+} of the pristine NCM cathode dropped rapidly at the end of charging (≥4.2 V) because of the shrinkage of Li slab along *c*-axis, thereby impeding the Li^+ de/intercalation. By comparing these two electrodes, we can draw that the D_{Li^+} value of NCM-Nb2 is about 3.5 times higher (~2.45×10^{-9} cm^2/s) than that of pristine NCM (~6.81×10^{-10} cm^2/s). This is because the expanded interlayer spacing owing to the doping of Nb^{5+} ions with a larger radius increases the mobility of Li^+ ions. Moreover, the forming of $LiNbO_3$ fast ion conductor can also promote the rapid transfer of Li-ions between the electrode material and the electrolyte. Therefore, the combined effect of both of the above improves the electrochemical reaction kinetics of the material.

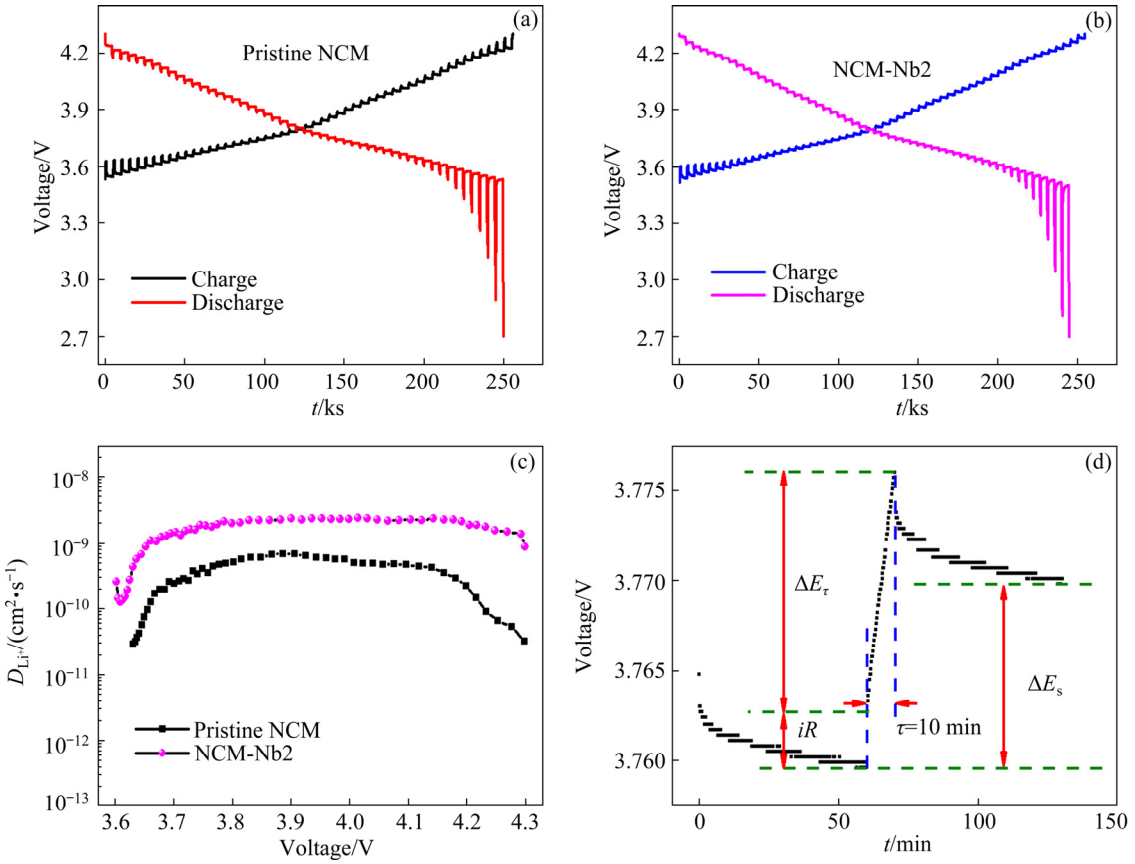

Fig. 10 GITT profiles of pristine NCM (a) and NCM-Nb2 (b) cathodes, obtained D_{Li^+} corresponding to charging procedure (c), and time vs voltage for single titration step of GITT profiles (d)

To reveal the kinetic characteristics of cathode materials, electrochemical impedance spectroscopy tests for pristine NCM and NCM-Nb2 were conducted. As shown in the possible equivalent circuit model in Fig. 11(a), each Nyquist plot contains two raised semicircles, representing the cathode−electrolyte interface resistance (R_{sf}) and the charge-transfer resistance (R_{ct}) from the high-frequency region to the medium-frequency region in turn, as well as a slope in the low-frequency region assigned to the Warburg impedance (W_o) related to the Li^+-ion diffusion kinetics [49]. Table 2 lists the impedance values of the pristine NCM and NCM-Nb2 cathodes fitted using the equivalent circuit. Compared with pristine NCM, the impedance value of NCM-Nb2 is remarkably reduced. After 100 cycles, the R_{sf} growth rate of NCM-Nb2 was apparently slower than that of pristine NCM, suggesting that the $LiNbO_3$ coating helped to form a more stable CEI layer. Similarly, the R_{ct} value of NCM-Nb2 also showed a more sluggish increment than pristine NCM, indicting a more excellent charge-transfer rate during electrochemical reaction process. This result is in accordance with the Li^+ diffusion coefficient tested by GITT. This is mainly because the $LiNbO_3$ interface coating with fast ionic conductivity can effectively suppress the adverse side reactions and reduce the impedance growth.

Thermal stability is one of the most key characteristic indexes of cathode materials, which directly determines the safety performance of the LIBs [50,51]. For this purpose, we used DSC to examine the pristine NCM and NCM-Nb2 cathodes at a fully charged state. The results are shown in Fig. 11(b). For the pristine NCM cathode, the exothermic peak temperature pointing to the interaction between the cathode and the electrolyte was only 227 °C, while NCM-Nb2 shifted to a higher temperature of 248 °C. In addition, the peak area of NCM-Nb2 associated with the heat generation of the exothermic reaction was remarkably reduced than that of pristine NCM. These phenomena may be ascribed to that Nb^{5+} ion doping and $LiNbO_3$ surface coating can simultaneously improve the overall structural stability of Ni-rich layered oxides from interface to bulk, and definitely inhibit the thermal effect between the highly delithiated cathode and the electrolyte.

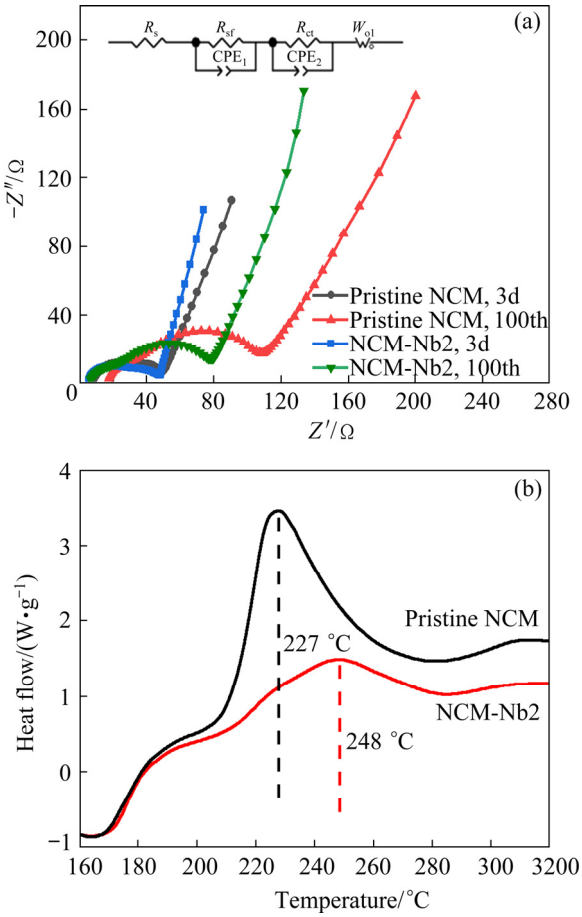

Fig. 11 Nyquist plots of cathodes after 3rd and 100th cycles (a), and DSC curves of cathodes after being fully charged at 4.3 V (b)

Table 2 Fitting parameters of impedance spectra after 3rd and 100th cycles

Sample	After 3rd cycle			After 100th cycle		
	R_s/Ω	R_{sf}/Ω	R_{ct}/Ω	R_s/Ω	R_{sf}/Ω	R_{ct}/Ω
Pristine-NCM	8.95	18.05	24.69	16.54	44.22	98.42
NCM-Nb2	5.53	16.69	21.52	6.98	34.86	56.61

4 Conclusions

(1) The dual-modified Ni-rich layered oxide cathode materials ($LiNi_{0.83}Co_{0.12}Mn_{0.05}O_2$) with Nb doping and $LiNbO_3$ surface coating were successfully synthesized through a simple but controllable one-step wet chemical method.

(2) The strong Nb—O bond can reduce Li^+/Ni^{2+} cation mixing and strengthen bulk structure. Meanwhile, the derived $LiNbO_3$ coating effectively stabilized the interface between the cathode material and the electrolyte, and facilitated the

diffusion of lithium ions. As a consequence, the dual-modified cathode materials exhibited improved overall structural stability and superior electrochemical performance compared to the pristine NCM, in terms of cycle stability, rate performance and thermodynamic properties.

(3) It can be inferred that this novel and effective strategy can also be extended to other oxide cathode materials for LIBs to synergistically improve the overall structural stability, and ultimately realize the excellent electrochemical performance.

Acknowledgments

This work was financially supported by the Regional Innovation and Development Joint Fund of National Natural Science Foundation of China (No. U19A2018), the National Natural Science Foundation of China (No. 21703191), Project of Innovation Team of the Ministry of Education, China (No. IRT_17R90), Hunan Provincial Natural Scientific Foundation of China (No. 2019JJ50600), and Outstanding Youth Project of Hunan Provincial Education Department, China (No. 18B076).

References

[1] KHAN I, BAIG N, ALI S, USMAN M, KHAN S A, SAEED K. Progress in layered cathode and anode nanoarchitectures for charge storage devices: Challenges and future perspective [J]. Energy Storage Materials, 2021, 35: 443−469.

[2] BIANCHINI M, ROCA-AYATS M, HARTMANN P, BREZESINSKI T, JANEK J. There and back again-the journey of $LiNiO_2$ as a cathode active material [J]. Angewandte Chemie (International Ed in English), 2019, 58(31): 10434−10458.

[3] LU Yong, ZHANG Yu-dong, ZHANG Qiu, CHENG Fang-yi, CHEN Jun. Recent advances in Ni-rich layered oxide particle materials for lithium-ion batteries [J]. Particuology, 2020, 53: 1−11.

[4] LIU Jun-xiang, WANG Jia-qi, NI You-xuan, ZHANG Kai, CHENG Fang-yi, CHEN Jun. Recent breakthroughs and perspectives of high-energy layered oxide cathode materials for lithium ion batteries [J]. Materials Today, 2021, 43: 132−165.

[5] YU Zhen-lu, QU Xing-yu, WAN Tao, DOU Ai-chun, ZHOU Yu, PENG Xiao-qi, SU Ming-ru, LIU Yun-jian, CHU De-wei. Synthesis and mechanism of high structural stability of nickel-rich cathode materials by adjusting Li-excess [J]. ACS Applied Materials & Interfaces, 2020, 12(36): 40393−40403.

[6] LU Shi-jie, LIU Yang, HE Zhen-jiang, LI Yun-jiao, ZHENG Jun-chao, MAO Jing, DAI Ke-hua. Synthesis and properties of single-crystal Ni-rich cathode materials in Li-ion batteries [J]. Transactions of Nonferrous Metals Society of China, 2021, 31(4): 1074−1086.

[7] LI Tian-yu, YUAN Xiao-Zi, ZHANG Lei, SONG Da-tong, SHI Kai-yuan, BOCK C. Degradation mechanisms and mitigation strategies of nickel-rich NMC-based lithium-ion batteries [J]. Electrochemical Energy Reviews, 2020, 3(1): 43−80.

[8] YIN Shou-yi, DENG Wen-tao, CHEN Jun, GAO Xu, ZOU Guo-qiang, HOU Hong-shuai, JI Xiao-bo. Fundamental and solutions of microcrack in Ni-rich layered oxide cathode materials of lithium-ion batteries [J]. Nano Energy, 2021, 83: 105854.

[9] ZHANG S S. Problems and their origins of Ni-rich layered oxide cathode materials [J]. Energy Storage Materials, 2020, 24: 247−254.

[10] LIN Qing-yun, GUAN Wen-hao, ZHOU Jian-bin, MENG Jie, HUANG Wei, CHEN Tao, GAO Qiang, WEI Xiao, ZENG Yue-wu, LI Ji-xue, ZHANG Ze. Ni-Li anti-site defect induced intragranular cracking in Ni-rich layer-structured cathode [J]. Nano Energy, 2020, 76: 105021.

[11] HWANG S, CHANG W, KIM S M, SU D, KIM D H, LEE J Y, CHUNG K Y, STACH E A. Investigation of changes in the surface structure of $Li_xNi_{0.8}Co_{0.15}Al_{0.05}O_2$ cathode materials induced by the initial charge [J]. Chemistry of Materials, 2014, 26(2): 1084−1092.

[12] BI Yu-jing, TAO Jin-hui, WU Yu-qin, LI Lin-ze, XU Yao-bin, HU En-yuan, WU Bing-bin, HU Jiang-tao, WANG Chong-min, ZHANG Ji-Guang, QI Yue, XIAO Jie. Reversible planar gliding and microcracking in a single-crystalline Ni-rich cathode [J]. Science, 2020, 370(6522): 1313−1317.

[13] MALEKI K S H, LI Xi-fei. Controllable cathode-electrolyte interface of $Li[Ni_{0.8}Co_{0.1}Mn_{0.1}]O_2$ for lithium ion batteries: A review [J]. Advanced Energy Materials, 2019, 9(39): 1901597.

[14] LIU Yuan, LIN Xi-Jie, SUN Yong-Gang, XU Yan-Song, CHANG Bao-Bao, LIU Chun-Tai, CAO An-Min, WAN Li-Jun. Precise surface engineering of cathode materials for improved stability of lithium-ion batteries [J]. Small, 2019, 15(32): e1901019.

[15] HAN Bing-hong, PAULAUSKAS T, KEY B, PEEBLES C, PARK J S, KLIE R F, VAUGHEY J T, DOGAN F. Understanding the role of temperature and cathode composition on interface and bulk: optimizing aluminum oxide coatings for Li-ion cathodes [J]. ACS Applied Materials & Interfaces, 2017, 9(17): 14769−14778.

[16] DAI Shi-can, YUAN Ming-liang, WANG Long, LUO Li-ming, CHEN Qi-chao, XIE Tang-feng, LI Ya-ping, YANG Yu-ting. Ultrathin-Y_2O_3-coated $LiNi_{0.8}Co_{0.1}Mn_{0.1}O_2$ as cathode materials for Li-ion batteries: Synthesis, performance and reversibility [J]. Ceramics International, 2019, 45(1): 674−680.

[17] XIONG Xun-hui, WANG Zhi-xing, YAN Guo-chun, GUO Hua-jun, LI Xin-hai. Role of V_2O_5 coating on $LiNiO_2$-based materials for lithium ion battery [J]. Journal of Power Sources, 2014, 245: 183−193.

[18] XIONG Xun-hui, WANG Zhi-xing, YIN Xing, GUO Hua-jun, LI Xin-hai. A modified LiF coating process to enhance the electrochemical performance characteristics of

$LiNi_{0.8}Co_{0.1}Mn_{0.1}O_2$ cathode materials [J]. Materials Letters, 2013, 110: 4−9.

[19] LIU Xue-ping, CHEN Quan-qi, LI Yan-wei, CHEN Chao, ZENG Wei, YUAN Min, WANG Ren-heng, XIAO Shun-hua. Synergistic modification of magnesium fluoride/sodium for improving the electrochemical performances of high-nickel ternary (NCM811) cathode materials [J]. Journal of the Electrochemical Society, 2019, 166(14): A3480−A3486.

[20] XIE Jin, SENDEK A D, CUBUK E D, ZHANG Xiao-kun, LU Zhi-yi, GONG Yong-ji, WU Tong, SHI Fei-fei, LIU Wei, REED E J, CUI Yi. Atomic layer deposition of stable $LiAlF_4$ lithium ion conductive interfacial layer for stable cathode cycling [J]. ACS Nano, 2017, 11(7): 7019−7027.

[21] FENG Ze, RAJAGOPALAN R, SUN Dan, TANG You-gen, WANG Hai-yan. In-situ formation of hybrid Li_3PO_4−$AlPO_4$−$Al(PO_3)_3$ coating layer on $LiNi_{0.8}Co_{0.1}Mn_{0.1}O_2$ cathode with enhanced electrochemical properties for lithium-ion battery [J]. Chemical Engineering Journal, 2020, 382: 122959.

[22] PENG Zhong-dong, LI Tian-fan, ZHANG Zhi-yong, DU Ke, HU Guo-rong, CAO Yan-bing. Surface architecture decoration on enhancing properties of $LiNi_{0.8}Co_{0.1}Mn_{0.1}O_2$ with building bi-phase Li_3PO_4 and AlPO4 by $Al(H_2PO_4)_3$ treatment [J]. Electrochimica Acta, 2020, 338: 135870.

[23] MIN K, PARK K, PARK S Y, SEO S W, CHOI B, CHO E. Improved electrochemical properties of $LiNi_{0.91}Co_{0.06}Mn_{0.03}O_2$ cathode material via Li-reactive coating with metal phosphates [J]. Scientific Reports, 2017, 7(1): 7151.

[24] XU Ya-Di, XIANG Wei, WU Zhen-guo, XU Chun-liu, LI Yong-chun, GUO Xiao-dong, LV Gen-pin, PENG Xi, ZHONG Ben-he. Improving cycling performance and rate capability of Ni-rich $LiNi_{0.8}Co_{0.1}Mn_{0.1}O_2$ cathode materials by $Li_4Ti_5O_{12}$ coating [J]. Electrochimica Acta, 2018, 268: 358−365.

[25] SCHIPPER F, BOUZAGLO H, DIXIT M, ERICKSON E M, WEIGEL T, TALIANKER M, GRINBLAT J, BURSTEIN L, SCHMIDT M, LAMPERT J, ERK C, MARKOVSKY B, MAJOR D T, AURBACH D. From surface ZrO_2 coating to bulk Zr doping by high temperature annealing of nickel-rich lithiated oxides and their enhanced electrochemical performance in lithium ion batteries [J]. Advanced Energy Materials, 2018, 8(4): 1701682.

[26] QU Xing-yu, YU Zhen-lu, RUAN Ding-shan, DOU Ai-chun, SU Ming-ru, ZHOU Yu, LIU Yun-jian, CHU De-wei. Enhanced electrochemical performance of ni-rich cathode materials with $Li_{1.3}Al_{0.3}Ti_{1.7}(PO_4)_3$ coating [J]. ACS Sustainable Chemistry & Engineering, 2020, 8(15): 5819−5830.

[27] ZHENG Jun-chao, YANG Zhuo, HE Zhen-jiang, TONG Hui, YU Wan-jing, ZHANG Jia-feng. In situ formed $LiNi_{0.8}Co_{0.15}Al_{0.05}O_2$@$Li_4SiO_4$ composite cathode material with high rate capability and long cycling stability for lithium-ion batteries [J]. Nano Energy, 2018, 53: 613−621.

[28] XIE Qiang, LI Wang-da, MANTHIRAM A. A Mg-doped high-nickel layered oxide cathode enabling safer, high-energy-density Li-ion batteries [J]. Chemistry of Materials, 2019, 31(3): 938−946.

[29] WEIGEL T, SCHIPPER F, ERICKSON E M, SUSAI F A, MARKOVSKY B, AURBACH D. Structural and electrochemical aspects of $LiNi_{0.8}Co_{0.1}Mn_{0.1}O_2$ cathode materials doped by various cations [J]. ACS Energy Letters, 2019, 4(2): 508−516.

[30] PARK K J, JUNG H G, KUO L Y, KAGHAZCHI P, YOON C S, SUN Y K. Improved cycling stability of $Li[Ni_{0.90}Co_{0.05}Mn_{0.05}]O_2$ through microstructure modification by boron doping for Li-ion batteries [J]. Advanced Energy Materials, 2018, 8(25): 1801202.

[31] KIM U H, JUN D W, PARK K J, ZHANG Q, KAGHAZCHI P, AURBACH D, MAJOR D T, GOOBES G, DIXIT M, LEIFER N, WANG C M, YAN P, AHN D, KIM K H, YOON C S, SUN Y K. Pushing the limit of layered transition metal oxide cathodes for high-energy density rechargeable Li ion batteries [J]. Energy & Environmental Science, 2018, 11(5): 1271−1279.

[32] XIA Yu, ZHENG Jian-ming, WANG Chong-min, GU Meng. Designing principle for Ni-rich cathode materials with high energy density for practical applications [J]. Nano Energy, 2018, 49: 434−452.

[33] QU Xing-yu, HUANG He, WAN Tao, HU Long, YU Zhen-lu, LIU Yun-jian, DOU Ai-chun, ZHOU Yu, SU Ming-ru, PENG Xiao-qi, WU Hong-Hui, WU T, CHU De-wei. An integrated surface coating strategy to enhance the electrochemical performance of nickel-rich layered cathodes [J]. Nano Energy, 2022, 91: 106665.

[34] LIU Si-yang, CHEN Xiang, ZHAO Jia-yue, SU Jun-ming, ZHANG Cong-cong, HUANG Tao, WU Jian-hua, YU Ai-shui. Uncovering the role of Nb modification in improving the structure stability and electrochemical performance of $LiNi_{0.6}Co_{0.2}Mn_{0.2}O_2$ cathode charged at higher voltage of 4.5 V [J]. Journal of Power Sources, 2018, 374: 149−157.

[35] XIN Feng-xia, ZHOU Hui, ZONG Yan-xu, ZUBA M, CHEN Yan, CHERNOVA N A, BAI Jian-ming, PEI Ben, GOEL A, RANA J, WANG Feng, AN Ke, PIPER L F J, ZHOU Guang-wen, WHITTINGHAM M S. What is the role of Nb in nickel-rich layered oxide cathodes for lithium-ion batteries? [J]. ACS Energy Letters, 2021, 6(4): 1377−1382.

[36] ZHOU Yu, LIU Ke, ZHOU Yue, NI Jia-hua, DOU Ai-chun, SU Ming-ru, LIU Yun-jian. Synthesis of a novel hexagonal porous TT-Nb_2O_5 via solid state reaction for high-performance lithium ion battery anodes [J]. Journal of Central South University, 2020, 27(12): 3625−3636.

[37] CHO Y, OH P, CHO J. A new type of protective surface layer for high-capacity Ni-based cathode materials: Nanoscaled surface pillaring layer [J]. Nano Letters, 2013, 13(3): 1145−1152.

[38] HUANG Yan, CAO Shuang, XIE Xin, WU Chao, JAMIL S, ZHAO Qing-lan, CHANG Bao-bao, WANG Ying, WANG Xian-you. Improving the structure and cycling stability of Ni-rich layered cathodes by dual modification of yttrium doping and surface coating [J]. ACS Appl Mater Interfaces, 2020, 12(17): 19483−19494.

[39] XU Chun-liu, XIANG Wei, WU Zhen-guo, XU Ya-di, LI Yong-chun, WANG Yuan, XIAO Yao, GUO Xiao-dong, ZHONG Ben-he. Highly stabilized Ni-rich cathode material with Mo induced epitaxially grown nanostructured hybrid surface for high-performance lithium-ion batteries [J]. ACS Applied Materials & Interfaces, 2019, 11(18): 16629−16638.

[40] ZUBAIR M, LI Guang-yin, WANG Bo-ya, WANG Lin, YU Hai-jun. Electrochemical kinetics and cycle stability improvement with Nb doping for lithium-rich layered oxides [J]. ACS Applied Energy Materials, 2019, 2(1): 503−512.

[41] LIU Yang, TANG Lin-bo, WEI Han-xin, ZHANG Xia-hui, HE Zhen-jiang, LI Yun-jiao, ZHENG Jun-chao. Enhancement on structural stability of Ni-rich cathode materials by in-situ fabricating dual-modified layer for lithium-ion batteries [J]. Nano Energy, 2019, 65: 104043.

[42] LI Xue-lei, JIN Liu-bing, SONG Da-wei, ZHANG Hong-zhou, SHI Xi-xi, WANG Zhen-yu, ZHANG Lian-qi, ZHU Ling-yun. $LiNbO_3$-coated $LiNi_{0.8}Co_{0.1}Mn_{0.1}O_2$ cathode with high discharge capacity and rate performance for all-solid-state lithium battery [J]. Journal of Energy Chemistry, 2020, 40: 39−45.

[43] KIM H, BYUN D, CHANG W, JUNG H G, CHOI W. A nano-$LiNbO_3$ coating layer and diffusion-induced surface control towards high-performance 5 V spinel cathodes for rechargeable batteries [J]. Journal of Materials Chemistry A, 2017, 5(47): 25077−25089.

[44] TANG Man-jing, YANG Jun, CHEN Nan-tao, ZHU Sheng-cai, WANG Xing, WANG Tian, ZHANG Cong-cong, XIA Yong-yao. Overall structural modification of a layered Ni-rich cathode for enhanced cycling stability and rate capability at high voltage [J]. Journal of Materials Chemistry A, 2019, 7(11): 6080−6089.

[45] ZHANG Xiao-yun, ZHANG Pan-pan, ZENG Tian-yi, YU Zhen-lu, QU Xing-yu, PENG Xiao-qi, ZHOU Yu, DUAN Xiao-guang, DOU Ai-chun, SU Ming-ru, LIU Yun-jian. Improving the structure stability of $LiNi_{0.8}Co_{0.15}Al_{0.05}O_2$ by double modification of tantalum surface coating and doping [J]. ACS Applied Energy Materials, 2021, 4(8): 8641−8652.

[46] PAN Cheng-chi, ZHU Yi-rong, YANG Ying-chang, HOU Hong-shuai, JING Ming-jun, SONG Wei-xin, YANG Xu-ming, JI Xiao-bo. Influences of transition metal on structural and electrochemical properties of $Li[Ni_xCo_yMn_z]O_2$ ($0.6\leq x\leq 0.8$) cathode materials for lithium-ion batteries [J]. Transactions of Nonferrous Metals Society of China, 2016, 26(5): 1396−1402.

[47] RYU H H, PARK K J, YOON C S, SUN Y K. Capacity fading of Ni-rich $Li[Ni_xCo_yMn_{1-x-y}]O_2$ ($0.6 \leq x \leq 0.95$) cathodes for high-energy-density lithium-ion batteries: Bulk or surface degradation? [J]. Chemistry of Materials, 2018, 30(3): 1155−1163.

[48] LI Hong-yang, LIU A, ZHANG Ning, WANG Yi-qiao, YIN Shuo, WU Hao-han, DAHN J R. An unavoidable challenge for Ni-rich positive electrode materials for lithium-ion batteries [J]. Chemistry of Materials, 2019, 31(18): 7574−7583.

[49] QIAN Rui-cheng, LIU Ya-li, CHENG Tao, LI Pan-pan, CHEN Ri-ming, LYU Ying-chun, GUO Bing-kun. Enhanced surface chemical and structural stability of Ni-rich cathode materials by synchronous lithium-ion conductor coating for lithium-ion batteries [J]. ACS Applied Materials & Interfaces, 2020, 12(12): 13813−13823.

[50] DONG Ming-xia, LI Xiang-qun, WANG Zhi-xing, LI Xin-hai, GUO Hua-jun, HUANG Zhen-jun. Enhanced cycling stability of La modified $LiNi_{0.8-x}Co_{0.1}Mn_{0.1}La_xO_2$ for Li-ion battery [J]. Transactions of Nonferrous Metals Society of China, 2017, 27(5): 1134−1142.

[51] ZENG Xiao-qiao, ZHAN Chun, LU Jun, AMINE K. Stabilization of a high-capacity and high-power nickel-based cathode for Li-ion batteries [J]. Chem, 2018, 4(4): 690−704.

一步双修饰策略提高富镍层状氧化物正极材料的电化学性能

曹远麟，杨秀康，王 璐，肖 玲，符 妮，邹 莉，
马温博，刘哲廷，王晓琴，刘 黎，舒洪波，王先友

湘潭大学 化学学院 湖南省电化学储能与转换重点实验室，
国家国际科技合作基地 环境友好化学与应用教育部重点实验室，湘潭 411105

摘 要：提出一种从表面到体相的一步整体改性策略，同步合成 Nb 掺杂和 $LiNbO_3$ 包覆的 $LiNi_{0.83}Co_{0.12}Mn_{0.05}O_2$ (NCM)正极材料。$LiNbO_3$ 包覆层可以调控界面并促进锂离子扩散；更强的 Nb—O 键能有效抑制 Li^+/Ni^{2+}阳离子混排，提高晶体结构稳定性，从而有助于缓解 Li^+脱出/嵌入过程中晶格参数的各向异性变化。结果表明：双修饰材料表现出较好的结构稳定性和优异的电化学性能。最佳样品 NCM-Nb2 在 2.7~4.3 V 之间以 1*C* 循环 100 次后，容量保持率为 90.78%，而原始样品容量保持率仅为 67.90%；同时，在 10*C* 下具有 149.1 mA·h/g 的更高倍率性能，这些结果突显了一步双修饰策略协同提高富镍层状氧化物正极材料电化学性能的可行性。

关键词：富镍正极材料；铌；一步策略；双重修饰；结构稳定性；电化学性能

(Edited by Xiang-qun LI)